Performance Analysis of Hybrid FSO/RF-THz Relay Communication System

Jingyuan Liang, Minghui Chen, and Xizheng Ke

***Abstract*—In the connection between the last kilometer access network and the backbone network, the dual-hop hybrid free-space optical/radio frequency(FSO/RF) relay system is considered to be an effective solution to increase the capacity and coverage of the wireless communication system. However, the transmission performance of FSO link is greatly affected by atmospheric turbulence, pointing errors and weather such as fog and snow, and the RF access network has low rate and relatively high delay. To ensure communication quality, a hybrid FSO/RF-terahertz(THz) relay system has been designed. Decode-and-forward relay is selected, and the hybrid FSO/RF communication based on adaptive combining scheme is considered before the relay node, and THz link is used after the relay node to access the users. Using the statistical characteristics of different links obtained, expressions for the outage probability and average bit error rate of the system were derived. The effects of different parameters on the performance of hybrid FSO/RF-THz relay system is studied, and the first hop adaptive combining scheme is compared with the single-threshold switching scheme and the single-link FSO system. The analysis results indicate that the hybrid FSO/RF-THz relay system can provide better outage and bit error rate performance by using the adaptive combining scheme, which can improve the system communication rate while taking into account the communication reliability.**

***Index Terms*—Free-space optical (FSO) communication, radio frequency (RF) communication, terahertz (THz) communication, adaptive combining scheme, relay performance analysis.**

I. Introduction

FREE-space optical (FSO) communications have received much attention in the field of wireless communications due to its advantages of high-speed rate, large capacity, strong confidentiality, low cost, and ease of deployment, making it the primary choice for connecting between radio frequency (RF) access networks and backbone networks. However, FSO is highly sensitive to problems such as atmospheric turbulence, pointing errors, and weather conditions (e.g., fog, haze, and snow), which limit the transmission distance of FSO links and seriously affect the performance of FSO communications [1], [2], [3]. On the other hand, RF communication, only attenuates severely in rain, is insensitive to atmospheric turbulence and pointing errors, and has strong environmental adaptability, but RF communication still has disadvantages such as poor interference resistance, low security, and low rate [4]. In addition, terahertz (THz) communication (0.1 THz -10 THz), as one of the core technologies of B5G and 6G communication, has a frequency band between RF and FSO, which has the advantages of low latency, high directional gain, and high available bandwidth, however, the huge path loss and molecular absorption, pointing errors and other problems lead to the limited transmission distance of THz communication, and thus THz is suitable for short-distance and high-speed communication [5], [6].

Given the advantages and disadvantages of FSO, RF, and THz communication mentioned above, hybrid communication has emerged to overcome the limitations of a single communication method in different scenarios and improve system performance. Hybrid communication is considered as a promising architecture in wireless communication and has received a lot of attention. Various types of hybrid systems have been studied in different works which can mainly be divided into two parts. The performance of hybrid relaying systems was studied in [7]-[13], and [9] derived exact expressions for the outage probability, bit error rate (BER), and ergodic capacity of hybrid FSO-RF systems using amplify-and-forward (AF) and decode-and-forward (DF) relaying, which provided a general framework for the performance analysis of the dual-hop hybrid FSO-RF system. [10] investigated the UAV-assisted asymmetric dual-hop hybrid FSO-RF system. [11] compared the performance of hybrid FSO-RF relay systems under the influence of intensity modulation/direct detection and heterodyne detection. At the same time, with the continuous development of THz technology, THz links have recently been introduced into hybrid relay systems. [12] analyzed the performance of hybrid THz-FSO relay system under the influence of pointing errors and channel fading. In [13], a hybrid RF-THz relay communication system with multiple antenna diversity is proposed. The performance of parallel hybrid systems was studied in [14]-[21], and literature [17] analyzed the effect of weather on hybrid networks with FSO links as primary links and RF links as backup links. [18] applied a rateless coding in hybrid FSO/RF system, which can fully utilize the FSO and RF channel resources. [19] proposed a hybrid FSO/RF communication system based on signal-to-noise ratio (SNR) threshold switching, but this method leads to frequent link switching between FSO and RF links. Therefore, a new hybrid FSO/RF system using adaptive combining scheme was

Manuscript received ; revised ; accepted . Date of publication ; date of current version . This work was supported by the National Natural Science Foundation of China under Grant 61377080. *(Corresponding authors: Xizheng Ke.)*

The authors are with College of Automation and Information Engineering, Xi'an University of Technology, Xi'an, Shaanxi 710048, China(e-mail: ljy@xaut.edu.cn; xzke@263.net).

Digital Object Identifier

proposed in [20] to solve the shortcomings of the method in [19]. [21] analyzed the hybrid FSO/RF system under the combined influence of pointing errors and atmospheric turbulence. In addition, [22] and [23] also investigated parallel multi-hop hybrid relay systems, which are equipped with both FSO and RF transceivers at each hop. Currently, the research on hybrid communication systems mainly focuses on the hybridization of FSO and RF, FSO and THz, and THz and RF. There are few reports on communication systems that mix FSO, RF, and THz simultaneously.

Combining the idea of parallel transmission mode of hybrid communication, this paper improves on the hybrid FSO/RF serial relay system and designs a hybrid FSO/RF-THz relay communication system, considering that the FSO link and THz link are modeled by the Gamma-Gamma and α-μ distributions with pointing errors, respectively, while the RF link follows the Nakagami-m distribution. The hybrid FSO/RF-THz relay communication system uses the hybrid FSO/RF communication based on adaptive combining scheme to alleviate the degradation of the system performance of the separate FSO link due to atmospheric turbulence and other factors, and after the relay node, the THz link is utilized instead of the traditional millimeter-wave RF link to access the user, thus further improving the system communication rate. The outage probability and average BER expressions of the system are derived, and the correctness of the derived performance formula is verified by simulating the relationship between different parameters and the performance of the hybrid FSO/RF-THz relay system.

II. System and Channel Models

A. System Model

The hybrid FSO/RF-THz relay system is shown in Fig.1, which is a dual-hop hybrid communication system that can provides users with high-speed rate, low latency, safe and reliable data transmission. Adopting DF relay mode, the communication distance from the source (S) node to the relay (R) node is relatively long. The hybrid FSO/RF communication system based on the adaptive combining scheme is adopted. The relay node R to the destination (D) node uses a short-distance THz link to access the users. Since FSO only supports line-of-sight communication and RF is used as a backup link for FSO in the hybrid FSO/RF-THz relay system, the transmitters and receivers of both FSO and RF link are deployed at the top of the building.

For the first hop S-R hybrid FSO/RF communication system based on adaptive combining scheme [24][7], when the instantaneous SNR γ_F of the FSO link receiver is higher than the set threshold γ_{th}, the signal is transmitted through the FSO link; when the instantaneous SNR γ_F of the FSO link drops below the set threshold γ_{th}, the receiver sends 1-bit feedback information to activate the RF link, and the communication rate of the FSO link is reduced to the RF link. The signal is transmitted simultaneously through the FSO link and the RF link, and the maximum ratio combiner is used to combine the signals received from the two links. Therefore, the combining rules of the hybrid FSO/RF communication system based on adaptive combining scheme can be expressed as

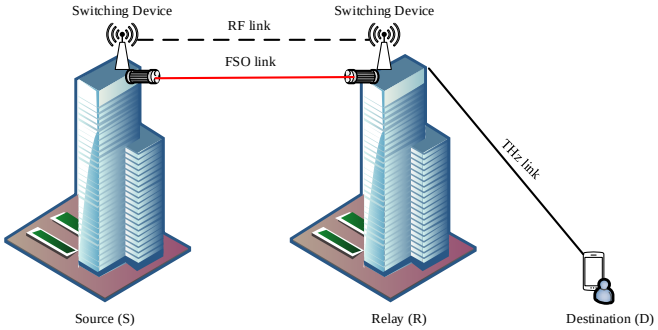

Fig. 1. Hybrid FSO/RF-THz relay system model.

$$\gamma_c = \begin{cases} \gamma_F, & \gamma_F \geq \gamma_{th} \\ \gamma_F + \gamma_R, & \gamma_F < \gamma_{th} \end{cases} \tag{1}$$

where γ_c is the output SNR of the adaptive combining scheme, γ_R is the instantaneous SNR of RF link.

B. FSO Link

Assuming that the FSO link adopts subcarrier intensity modulation (SIM) and direct detection technology, the optical signal received at the relay R can be expressed as

$$y_F = P_F \eta I_l I x + n_F \tag{2}$$

where P_F is the transmission power of the FSO link, η denotes the photoelectric conversion coefficient, I_l denotes the atmospheric attenuation associated with the FSO link, according to Beer-Lambert law $I_l = \exp(-\sigma_l L_F)$, σ_l is the attenuation coefficient, and L_F is the FSO link distance. x represents the signal transmitted at the source node S, n_F represents the additive white Gaussian noise with mean 0 and variance σ_F^2 of the FSO link, and $I = I_a I_p$ represents the effective channel gain of the FSO link, including atmospheric turbulence I_a and pointing errors I_p.

The FSO link fading I_a caused by turbulence follows a Gamma-Gamma distribution, then the probability density function (PDF) of I_a is

$$f_{I_a}(x) = \frac{2x^{-1}}{\Gamma(\alpha_F)\Gamma(\beta_F)} G_{0\,2}^{2\,0}(\alpha_F \beta_F x|_{\alpha_F, \beta_F}^{-}) \tag{3}$$

where $\Gamma(\cdot)$ represents Gamma function, $G_{p,q}^{m,n}(\cdot)$ denotes Meijer-G function, The large-scale turbulence coefficient β_F and the small-scale turbulence coefficient α_F are given as

$$\begin{cases} \alpha_F = \left[\exp\left(\dfrac{0.49\sigma_{RV}^2}{(1+1.11\sigma_{RV}^{12/5})^{7/6}} \right) - 1 \right]^{-1} \\ \beta_F = \left[\exp\left(\dfrac{0.51\sigma_{RV}^2}{(1+0.69\sigma_{RV}^{12/5})^{5/6}} \right) - 1 \right]^{-1} \end{cases} \tag{4}$$

in (4), $\sigma_{\mathrm{RV}}^2=1.23C_n^2k_0^{7/6}L_{\mathrm{F}}^{11/6}$ is the Rytov variance, where the wavenumber $k_0=2\pi/\lambda_{\mathrm{F}}$, C_n^2 represents the atmospheric refractive index structure constant.

$I_{\mathrm{p}}\approx A_{0,\mathrm{F}}\exp(-2r^2/w_{L_{\mathrm{eq}}}^2)$ is the fading coefficient caused by the pointing error during the FSO link transmission [25][25], where r represents the radial displacement between the beam center and the detector, r follows the modified Rayleigh distribution, $A_{0,\mathrm{F}}$ represents part of the received optical power at r=0, $A_{0,\mathrm{F}}=\mathrm{erf}^2(v)$, $v=\sqrt{\frac{\pi}{2}}\frac{r_{\mathrm{a}}}{w_L}$, r_{a} denotes the aperture radius, w_L denotes the beam width, $w_{L_{\mathrm{eq}}}$ is the equivalent beam width, $w_{L_{\mathrm{eq}}}^2=\frac{w_L^2\sqrt{\pi}\,\mathrm{erf}(v)}{2v\exp(-v^2)}$. Therefore, considering the zero-axis pointing error, the PDF of I_{p} can be represented as

$$f_{I_{\mathrm{p}}}(x)=\frac{\xi_{\mathrm{F}}^2}{A_{0,\mathrm{F}}^{\xi_{\mathrm{F}}^2}}x^{\xi_{\mathrm{F}}^2-1},\ 0\le x\le A_{0,\mathrm{F}} \tag{5}$$

where $\xi_{\mathrm{F}}=\frac{w_{L_{\mathrm{eq}}}}{2\sigma_{\mathrm{j,F}}}$ denotes FSO link pointing error coefficient, $\sigma_{\mathrm{j,F}}$ denotes the jitter standard deviation of FSO link.

From $f_I(I)=\int f_{I|I_{\mathrm{a}}}(I\mid I_{\mathrm{a}})f_{I_{\mathrm{a}}}(I_{\mathrm{a}})\mathrm{d}I_{\mathrm{a}}$, we get the PDF of the effective channel gain I of the FSO link under the combined influence of atmospheric turbulence and pointing error as

$$f_I(I)=\frac{\alpha_{\mathrm{F}}\beta_{\mathrm{F}}\xi_{\mathrm{F}}^2}{A_{0,\mathrm{F}}I_1\Gamma(\alpha_{\mathrm{F}})\Gamma(\beta_{\mathrm{F}})}G_{1,3}^{3,0}\left[\frac{\alpha_{\mathrm{F}}\beta_{\mathrm{F}}I}{A_{0,\mathrm{F}}I_1}\middle|_{\xi_{\mathrm{F}}^2-1,\alpha_{\mathrm{F}}-1,\beta_{\mathrm{F}}-1}^{\xi_{\mathrm{F}}^2}\right] \tag{6}$$

Since the instantaneous SNR and average SNR of the FSO link are $\gamma_{\mathrm{F}}=\frac{|I|^2P_{\mathrm{F}}^2\eta^2}{\sigma_{\mathrm{F}}^2}$ and $\bar{\gamma}_{\mathrm{F}}=\frac{P_{\mathrm{F}}^2\eta^2\xi_{\mathrm{F}}^4}{\sigma_{\mathrm{F}}^2(\xi_{\mathrm{F}}^2+1)^2}A_{0,\mathrm{F}}^2I_1^2$, respectively, using γ_{F} and $\bar{\gamma}_{\mathrm{F}}$ to replace the variable I in (6) can obtain the PDF of γ_{F} as [26], [27]

$$f_{\gamma_{\mathrm{F}}}(x)=\frac{\xi_{\mathrm{F}}^2}{2\Gamma(\alpha_{\mathrm{F}})\Gamma(\beta_{\mathrm{F}})x}G_{1,3}^{3,0}\left[\frac{\alpha_{\mathrm{F}}\beta_{\mathrm{F}}\xi_{\mathrm{F}}^2}{\xi_{\mathrm{F}}^2+1}\left(\frac{x}{\bar{\gamma}_{\mathrm{F}}}\right)^{\frac{1}{2}}\middle|_{\xi_{\mathrm{F}}^2,\alpha_{\mathrm{F}},\beta_{\mathrm{F}}}^{\xi_{\mathrm{F}}^2+1}\right] \tag{7}$$

By integrating (7), the cumulative distribution function (CDF) of γ_f can be obtained as

$$F_{\gamma_{\mathrm{F}}}(x)=\frac{2^{\alpha_{\mathrm{F}}+\beta_{\mathrm{F}}-3}\xi_{\mathrm{F}}^2}{\pi\Gamma(\alpha_{\mathrm{F}})\Gamma(\beta_{\mathrm{F}})}\times G_{3,7}^{6,1}\left(\frac{\alpha_{\mathrm{F}}^2\beta_{\mathrm{F}}^2\xi_{\mathrm{F}}^4x}{16(\xi_{\mathrm{F}}^2+1)^2\bar{\gamma}_{\mathrm{F}}}\middle|_{\frac{\xi_{\mathrm{F}}^2}{2},\frac{\xi_{\mathrm{F}}^2+1}{2},\frac{\alpha_{\mathrm{F}}}{2},\frac{\alpha_{\mathrm{F}}+1}{2},\frac{\beta_{\mathrm{F}}}{2},\frac{\beta_{\mathrm{F}}+1}{2},0}^{1,\frac{\xi_{\mathrm{F}}^2+1}{2},\frac{\xi_{\mathrm{F}}^2+2}{2}}\right) \tag{8}$$

C. RF Link

The received signal of RF link at relay R can be expressed as

$$y_{\mathrm{R}}=\sqrt{P_{\mathrm{R}}h_{\mathrm{l,R}}}h_{\mathrm{R}}x+n_{\mathrm{R}} \tag{9}$$

where P_{R} is the transmit power of the RF link, $h_{\mathrm{l,R}}=G_{\mathrm{t,R}}+G_{\mathrm{r,R}}-20\lg(\frac{4\pi L_{\mathrm{R}}}{\lambda_{\mathrm{R}}})-(\alpha_{\mathrm{oxy}}+\alpha_{\mathrm{rain}})L_{\mathrm{R}}$ denotes the path loss of the RF link, $G_{\mathrm{t,R}}$ and $G_{\mathrm{r,R}}$ represent the gain of RF link transmitting antenna and receiving antenna, respectively, L_{R} and λ_{R} are the RF link distance and wavelength, respectively, α_{oxy} and α_{rain} are the attenuation coefficient caused by oxygen and rain absorption, respectively. h_{R} is the fading coefficient of the RF link, which follows the Nakagmi-m distribution, and n_{R} is the additive Gaussian white noise with mean 0 and variance σ_{R}^2 of the RF link.

The instantaneous SNR and average SNR received by the RF link are $\gamma_{\mathrm{R}}=\bar{\gamma}_{\mathrm{R}}|h_{\mathrm{R}}|^2$ and $\bar{\gamma}_{\mathrm{R}}=\frac{P_{\mathrm{R}}h_{\mathrm{l,R}}}{\sigma_{\mathrm{R}}^2}$, respectively, so the PDF of γ_{R} can be written as [28]

$$f_{\gamma_{\mathrm{R}}}(x)=\left(\frac{m}{\bar{\gamma}_{\mathrm{R}}}\right)^m\frac{x^{m-1}}{\Gamma(m)}\exp\left(-\frac{mx}{\bar{\gamma}_{\mathrm{R}}}\right) \tag{10}$$

where m denotes the parameter of channel fading degree.

By integrating (10), the CDF of γ_{R} can be obtained as

$$F_{\gamma_{\mathrm{R}}}(x)=\frac{1}{\Gamma(m)}\gamma\left(m,\frac{mx}{\bar{\gamma}_{\mathrm{R}}}\right) \tag{11}$$

where $\gamma(\cdot,\cdot)$ denotes the lower bound incomplete Gamma function.

D. THz Link

If the relay node R adopts DF relay forwarding mode, then the received signal at destination node D for the second hop THz link is

$$y_{\mathrm{T}}=\sqrt{P_{\mathrm{T}}}h_{\mathrm{l,T}}h_{\mathrm{T}}\hat{x}+n_{\mathrm{T}} \tag{12}$$

where P_{T} represents the transmit power of the THz link, $h_{\mathrm{l,T}}=\frac{c\sqrt{G_{\mathrm{t,T}}G_{\mathrm{r,T}}}}{4\pi f_{\mathrm{T}}L_{\mathrm{T}}}\exp[-\frac{1}{2}\kappa_a(f_{\mathrm{T}})L_{\mathrm{T}}]$ is the path loss of THz link, c is the speed of light, $G_{\mathrm{t,T}}$ and $G_{\mathrm{r,T}}$ denote the gains of THz link transmitting antenna and receiving antenna, respectively, f_{T} and L_{T} are the frequency and link distance of the THz link, respectively, $\kappa_a(\cdot)$ denotes the absorption coefficient with respect to temperature, relative humidity and atmospheric pressure, $\hat{x}$ denotes the decoded signal at the relay R, n_{T} denotes the additive Gaussian white noise with mean 0 and variance σ_{T}^2 of the THz link, and $h_{\mathrm{T}}=h_{\mathrm{p}}h_{\mathrm{f}}$ denotes the THz link channel coefficient, including the pointing error h_{p} and the channel fading h_{f}.

The THz link channel coefficients h_{T} experience α-μ fading with pointing error impairments. Therefore, considering the combined effects of channel fading and pointing error, the PDF of h_{T} is given by

$$f_{h_{\mathrm{T}}}(h_{\mathrm{T}})=\frac{\xi_{\mathrm{T}}^2\mu^{\frac{\xi_{\mathrm{T}}^2}{\alpha}}h_{\mathrm{T}}^{\xi_{\mathrm{T}}^2-1}}{A_{0,\mathrm{T}}^{\xi_{\mathrm{T}}^2}\Omega^{\xi_{\mathrm{T}}^2}\Gamma(\mu)}\Gamma(\frac{\alpha\mu-\xi_{\mathrm{T}}^2}{\alpha},\frac{\mu h_{\mathrm{T}}^{\alpha}}{A_{0,\mathrm{T}}^{\alpha}\Omega^{\alpha}}) \tag{13}$$

where ξ_{T} and $A_{0,\mathrm{T}}$ represent the THz link pointing error parameter and the partially received optical power, respectively, and their solution method refers to the FSO link pointing error parameter ξ_{F} and the partially received optical power $A_{0,\mathrm{F}}$. α and μ denote the channel fading parameters, Ω is the α-root mean of the fading channel envelope, $\Gamma(\cdot,\cdot)$ represents the upper bound incomplete Gamma function.

The instantaneous SNR received by the THz link is $\gamma_{\mathrm{T}}=\bar{\gamma}_{\mathrm{T}}\left|h_{\mathrm{T}}\right|^2$, and the average SNR of the THz link is $\bar{\gamma}_{\mathrm{T}}=\frac{P_{\mathrm{T}}h_{l,\mathrm{T}}^2}{\sigma_{\mathrm{T}}^2}$, so using γ_{T} and $\bar{\gamma}_{\mathrm{T}}$ for variable substitution of h_{T} in (13), the PDF of γ_{T} can be obtained as [29]

$$f_{\gamma_{\mathrm{T}}}(x)=\frac{\xi_{\mathrm{T}}^2\mu^{\frac{\xi_{\mathrm{T}}^2}{\alpha}}x^{\frac{\xi_{\mathrm{T}}^2}{2}-1}}{2A_{0,\mathrm{T}}^{\xi_{\mathrm{T}}^2}\Omega^{\xi_{\mathrm{T}}^2}\Gamma(\mu)\bar{\gamma}_{\mathrm{T}}^{\frac{\xi_{\mathrm{T}}^2}{2}}}\Gamma(\frac{\alpha\mu-\xi_{\mathrm{T}}^2}{\alpha},\frac{\mu x^{\frac{\alpha}{2}}}{A_{0,\mathrm{T}}^{\alpha}\Omega^{\alpha}\bar{\gamma}_{\mathrm{T}}^{\frac{\alpha}{2}}}) \tag{14}$$

By integrating (14), the CDF of γ_{T} can be obtained as

$$F_{\gamma_{\mathrm{T}}}(x)=\frac{\xi_{\mathrm{T}}^2\mu^{\frac{\xi_{\mathrm{T}}^2}{\alpha}}x^{\frac{\xi_{\mathrm{T}}^2}{2}}}{\alpha A_{0,\mathrm{T}}^{\xi_{\mathrm{T}}^2}\Omega^{\xi_{\mathrm{T}}^2}\Gamma(\mu)\bar{\gamma}_{\mathrm{T}}^{\frac{\xi_{\mathrm{T}}^2}{2}}}G_{2,3}^{2,1}\left[\frac{\mu x^{\frac{\alpha}{2}}}{A_{0,\mathrm{T}}^{\alpha}\Omega^{\alpha}\bar{\gamma}_{\mathrm{T}}^{\frac{\alpha}{2}}}\middle|_{0,\frac{\alpha\mu-\xi_{\mathrm{T}}^2}{\alpha},-\frac{\xi_{\mathrm{T}}^2}{\alpha}}^{1-\frac{\xi_{\mathrm{T}}^2}{\alpha},1}\right] \tag{15}$$

III. Performance Analysis

A. Outage Probability

The outage probability refers to the probability that the end-to-end (E2E) SNR of the communication system is lower than the set threshold [30], [31]. Therefore, in the first hop S-R hybrid FSO/RF communication system based on adaptive combining scheme, when the instantaneous SNR γ_{c} of the output after adaptive combining is lower than the preset outage threshold γ_{out}, the system is in an outage state, whose the outage probability can be expressed as $P_{\mathrm{out,AC}}=F_{\gamma_{\mathrm{c}}}(\gamma_{\mathrm{out}})=\Pr[\gamma_{\mathrm{c}}<\gamma_{\mathrm{out}}]$ .According to (1), the outage probability of hybrid FSO/RF communication system based on adaptive combining scheme can be expressed as

$$\begin{aligned}P_{\mathrm{out,AC}}&=F_{\gamma_{\mathrm{c}}}(x)\\&=\Pr[\gamma_{\mathrm{F}}\ge\gamma_{\mathrm{th}},\gamma_{\mathrm{F}}<x]+\Pr[\gamma_{\mathrm{F}}<\gamma_{\mathrm{th}},\gamma_{\mathrm{F}}+\gamma_{\mathrm{R}}<x]\\&=\begin{cases}F_1(x), & x\le\gamma_{\mathrm{th}}\\ F_2(x)-F_{\gamma_{\mathrm{F}}}(\gamma_{\mathrm{th}})+F_{\gamma_{\mathrm{F}}}(x), & x>\gamma_{\mathrm{th}}\end{cases}\end{aligned} \tag{16}$$

where $F_1(x)=\int_0^x f_{\gamma_{\mathrm{F}}+\gamma_{\mathrm{R}}}(t)\,\mathrm{d}t$, $F_2(x)=\int_0^{\gamma_{\mathrm{th}}} f_{\gamma_{\mathrm{F}}}(t)F_{\gamma_{\mathrm{R}}}(x-t)\,\mathrm{d}t$. Since the FSO link and the RF link are statistically independent, $f_{\gamma_{\mathrm{F}}+\gamma_{\mathrm{R}}}(x)=\int_0^x f_{\gamma_{\mathrm{F}}}(t)\,f_{\gamma_{\mathrm{R}}}(x-t)\,\mathrm{d}t$, substituting (7) and (10) into the calculation to get

$$\begin{aligned}f_{\gamma_{\mathrm{F}}+\gamma_{\mathrm{R}}}(x)=&\frac{2^{\alpha_{\mathrm{F}}+\beta_{\mathrm{F}}-3}\xi_{\mathrm{F}}^2}{\pi\Gamma(\alpha_{\mathrm{F}})\Gamma(\beta_{\mathrm{F}})\Gamma(m)}(\frac{m}{\bar{\gamma}_{\mathrm{R}}})^m x^{m-1}\\&\times\sum_{n=0}^{\infty}(-1)^n\frac{1}{n!}(\frac{m}{\bar{\gamma}_{\mathrm{R}}})^n\Gamma(m+n)x^n\\&\times G_{3,7}^{6,1}\left(\frac{\alpha_{\mathrm{F}}^2\beta_{\mathrm{F}}^2\xi_{\mathrm{F}}^4x}{16(\xi_{\mathrm{F}}^2+1)^2\bar{\gamma}_{\mathrm{F}}}\middle|_{\frac{\xi_{\mathrm{F}}^2}{2},\frac{\xi_{\mathrm{F}}^2+1}{2},\frac{\alpha_{\mathrm{F}}}{2},\frac{\alpha_{\mathrm{F}}+1}{2},\frac{\beta_{\mathrm{F}}}{2},\frac{\beta_{\mathrm{F}}+1}{2},1-m-n}^{1,\frac{\xi_{\mathrm{F}}^2+1}{2},\frac{\xi_{\mathrm{F}}^2+2}{2}}\right)\end{aligned} \tag{17}$$

then substituting (17), (7) and (11) into the expression of $F_1(x)$ and $F_2(x)$, respectively, to obtain

$$\begin{aligned}F_1(x)=&\frac{2^{\alpha_{\mathrm{F}}+\beta_{\mathrm{F}}-3}\xi_{\mathrm{F}}^2}{\pi\Gamma(\alpha_{\mathrm{F}})\Gamma(\beta_{\mathrm{F}})\Gamma(m)}(\frac{m}{\bar{\gamma}_{\mathrm{R}}})^m\\&\times\sum_{n=0}^{\infty}(-1)^n\frac{1}{n!}(\frac{m}{\bar{\gamma}_{\mathrm{R}}})^n\Gamma(m+n)x^{n+m}\\&\times G_{4,8}^{6,2}\left(\frac{\alpha_{\mathrm{F}}^2\beta_{\mathrm{F}}^2\xi_{\mathrm{F}}^4x}{16(\xi_{\mathrm{F}}^2+1)^2\bar{\gamma}_{\mathrm{F}}}\middle|_{\frac{\xi_{\mathrm{F}}^2}{2},\frac{\xi_{\mathrm{F}}^2+1}{2},\frac{\alpha_{\mathrm{F}}}{2},\frac{\alpha_{\mathrm{F}}+1}{2},\frac{\beta_{\mathrm{F}}}{2},\frac{\beta_{\mathrm{F}}+1}{2},1-m-n,-n-m}^{1-n-m,1,\frac{\xi_{\mathrm{F}}^2+1}{2},\frac{\xi_{\mathrm{F}}^2+2}{2}}\right)\end{aligned} \tag{18}$$

$$\begin{aligned}F_2(x)=&F_{\gamma_{\mathrm{F}}}(\gamma_{\mathrm{th}})-\frac{2^{\alpha_{\mathrm{F}}+\beta_{\mathrm{F}}-3}\xi_{\mathrm{F}}^2}{\pi\Gamma(\alpha_{\mathrm{F}})\Gamma(\beta_{\mathrm{F}})}e^{-\frac{mx}{\bar{\gamma}_{\mathrm{R}}}}\\&\times\sum_{n=0}^{\infty}\frac{1}{n!}(\frac{m\gamma_{\mathrm{th}}}{\bar{\gamma}_{\mathrm{R}}})^n\sum_{k=0}^{m-1}\frac{1}{k!}(\frac{mx}{\bar{\gamma}_{\mathrm{R}}})^k\sum_{j=0}^{k}\binom{k}{j}\left(\frac{-\gamma_{\mathrm{th}}}{x}\right)^j\\&\times G_{3,7}^{6,1}\left(\frac{\alpha_{\mathrm{F}}^2\beta_{\mathrm{F}}^2\xi_{\mathrm{F}}^4\gamma_{\mathrm{th}}}{16(\xi_{\mathrm{F}}^2+1)^2\bar{\gamma}_{\mathrm{F}}}\middle|_{\frac{\xi_{\mathrm{F}}^2}{2},\frac{\xi_{\mathrm{F}}^2+1}{2},\frac{\alpha_{\mathrm{F}}}{2},\frac{\alpha_{\mathrm{F}}+1}{2},\frac{\beta_{\mathrm{F}}}{2},\frac{\beta_{\mathrm{F}}+1}{2},-n-j}^{1-n-j,\frac{\xi_{\mathrm{F}}^2+1}{2},\frac{\xi_{\mathrm{F}}^2+2}{2}}\right)\end{aligned} \tag{19}$$

Considering DF relay, E2E outage probability of hybrid FSO/RF-THz relay communication system can be written as

$$P_{\mathrm{out}}=1-(1-P_{\mathrm{out,AC}})\times(1-P_{\mathrm{out,T}}) \tag{20}$$

where $P_{\mathrm{out,T}}$ denotes the outage probability of the second hop R-D THz link, $P_{\mathrm{out,T}}=F_{\gamma_{\mathrm{T}}}(x)$. Thus, (20) can also be expressed as $P_{\mathrm{out}}=F_{\gamma_{\mathrm{c}}}(x)+F_{\gamma_{\mathrm{T}}}(x)-F_{\gamma_{\mathrm{c}}}(x)\times F_{\gamma_{\mathrm{T}}}(x)$, and the outage probability of the system can be obtained by substituting (15) and (16).

B. Average BER

According to the definition [32], the average BER of the communication system can be expressed as $\bar{P}_{\mathrm{e}}=\int_0^{\infty}P(\mathrm{e}\,|\,x)f_{\gamma}(x)\,\mathrm{d}\,x$, where $P(\mathrm{e}|x)$ denotes the conditional error probability corresponding to different modulation schemes. Therefore, assuming that the multiple phase shift keying (MPSK) modulation scheme is adopted, $P(\mathrm{e}\,|\,x)\approx\frac{A}{2}\mathrm{erfc}(\sqrt{x}B)$, the average BER of the first hop S-R hybrid FSO/RF communication system based on the adaptive combining scheme is given by

$$\bar{P}_{\mathrm{e,AC}}=\int_0^{\infty}\frac{A}{2}\mathrm{erfc}(\sqrt{x}B)f_{\gamma_{\mathrm{c}}}(x)\,\mathrm{d}\,x \tag{21}$$

where $B=\sin(\pi/M)$,when M=2(BPSK), A=1; when M>2,

A=2.

By differentiating (16), the PDF of γ_c can be obtained as

$$f_{\gamma_c}(x)=\begin{cases} f_{\gamma_F+\gamma_R}(x), & x\le\gamma_{th} \\ f_{\gamma_F}(x)+G(x), & x>\gamma_{th} \end{cases} \tag{22}$$

where $G(x)=\int_0^{\gamma_{th}} f_{\gamma_F}(t)f_{\gamma_R}(x-t)\,\mathrm{d}t$, substituting (7) and (10) into the calculation to get

$$\begin{aligned} G(x)=&\frac{2^{\alpha_F+\beta_F-3}\xi_F^2}{\pi\Gamma(\alpha_F)\Gamma(\beta_F)\Gamma(m)}\left(\frac{m}{\overline{\gamma}_R}x\right)^m \\ &\times\sum_{i=0}^{\infty}\frac{1}{i!}\left(-\frac{m}{\overline{\gamma}_R}x\right)^i\sum_{j=0}^{m+i-1}\frac{(-\gamma_{th})^j}{x^{j+1}}\binom{m+i-1}{j} \\ &\times G_{3,7}^{6,1}\left(\frac{\alpha_F^2\beta_F^2\xi_F^4\gamma_{th}}{16(\xi_F^2+1)^2\overline{\gamma}_F}\middle|\begin{matrix}1-j,\frac{\xi_F^2+1}{2},\frac{\xi_F^2+2}{2}\\ \frac{\xi_F^2}{2},\frac{\xi_F^2+1}{2},\frac{\alpha_F}{2},\frac{\alpha_F+1}{2},\frac{\beta_F}{2},\frac{\beta_F+1}{2},-j\end{matrix}\right) \end{aligned} \tag{23}$$

then, substituting (22) into (21) to obtain

$$\begin{aligned} \overline{P}_{e,AC}=&\underbrace{\int_0^{\gamma_{th}}\frac{A}{2}\mathrm{erfc}(\sqrt{x}B)f_{\gamma_F+\gamma_R}(x)\,\mathrm{d}x}_{I_1} \\ &+\underbrace{\int_{\gamma_{th}}^{\infty}\frac{A}{2}\mathrm{erfc}(\sqrt{x}B)\left[f_{\gamma_F}(x)+G(x)\right]\mathrm{d}x}_{I_2} \end{aligned} \tag{24}$$

Since erfc(x)=1-erf(x), the first term I_1 in (24) can be expressed as

$$I_1=\frac{A}{2}\left[\underbrace{\int_0^{\gamma_{th}}f_{\gamma_F+\gamma_R}(x)\,\mathrm{d}x}_{F_1(\gamma_{th})}-\underbrace{\int_0^{\gamma_{th}}\mathrm{erf}(\sqrt{x}B)f_{\gamma_F+\gamma_R}(x)\,\mathrm{d}x}_{I_{11}}\right] \tag{25}$$

substituting (17) into the expression of I_{11} in (25) to get

$$\begin{aligned} I_{11}=&\frac{2^{\alpha_F+\beta_F-2}\xi_F^2}{\pi^{3/2}\Gamma(\alpha_F)\Gamma(\beta_F)\Gamma(m)}\left(\frac{m\gamma_{th}}{\overline{\gamma}_R}\right)^m \\ &\times\sum_{n=0}^{\infty}\frac{(-1)^n(B\sqrt{\gamma_{th}})^{2n+1}}{n!(2n+1)}\sum_{k=0}^{\infty}\frac{(-1)^k}{k!}\left(\frac{m\gamma_{th}}{\overline{\gamma}_R}\right)^k\Gamma(m+k) \\ &\times G_{4,8}^{6,2}\left(\frac{\alpha_F^2\beta_F^2\xi_F^4\gamma_{th}}{16(\xi_F^2+1)^2\overline{\gamma}_F}\middle|\begin{matrix}\frac{1}{2}-n-m-k,1,\frac{\xi_F^2+1}{2},\frac{\xi_F^2+2}{2}\\ \frac{\xi_F^2}{2},\frac{\xi_F^2+1}{2},\frac{\alpha_F}{2},\frac{\alpha_F+1}{2},\frac{\beta_F}{2},\frac{\beta_F+1}{2},1-k-m,-n-k-m-\frac{1}{2}\end{matrix}\right) \end{aligned} \tag{26}$$

therefore, I_1 can be obtained by substituting (18) and (26) into (25).

Similarly, the second term I_2 in (24) can be expressed as

$$\begin{aligned} I_2=&\underbrace{\int_0^{\infty}\frac{A}{2}\mathrm{erfc}(\sqrt{x}B)f_{\gamma_F}(x)\,\mathrm{d}x}_{\overline{P}_{e,F}}-\frac{A}{2}\underbrace{\int_0^{\gamma_{th}}f_{\gamma_F}(x)\,\mathrm{d}x}_{F_{\gamma_F}(\gamma_{th})} \\ &+\underbrace{\int_0^{\gamma_{th}}\frac{A}{2}\mathrm{erf}(\sqrt{x}B)f_{\gamma_F}(x)\,\mathrm{d}x}_{I_{21}}+\underbrace{\int_{\gamma_{th}}^{\infty}\frac{A}{2}\mathrm{erfc}(\sqrt{x}B)G(x)\,\mathrm{d}x}_{I_{22}} \end{aligned} \tag{27}$$

substituting (7) and (23) into the expressions of $\overline{P}_{e,F}$, I_{21} and I_{22} in (27), respectively, and we get

$$\begin{aligned} \overline{P}_{e,F}=&\frac{2^{\alpha_F+\beta_F-4}A\xi_F^2}{\pi^{3/2}\Gamma(\alpha_F)\Gamma(\beta_F)} \\ &\times G_{4,7}^{6,2}\left(\frac{\alpha_F^2\beta_F^2\xi_F^4}{16B^2(\xi_F^2+1)^2\overline{\gamma}_F}\middle|\begin{matrix}1,\frac{1}{2},\frac{\xi_F^2+1}{2},\frac{\xi_F^2+2}{2}\\ \frac{\xi_F^2}{2},\frac{\xi_F^2+1}{2},\frac{\alpha_F}{2},\frac{\alpha_F+1}{2},\frac{\beta_F}{2},\frac{\beta_F+1}{2},0\end{matrix}\right) \end{aligned} \tag{28}$$

$$\begin{aligned} I_{21}=&\frac{2^{\alpha_F+\beta_F-3}A\xi_F^2}{\pi^{3/2}\Gamma(\alpha_F)\Gamma(\beta_F)}\sum_{n=0}^{\infty}\frac{(-1)^n(B\sqrt{\gamma_{th}})^{2n+1}}{n!(2n+1)} \\ &\times G_{3,7}^{6,1}\left(\frac{\alpha_F^2\beta_F^2\xi_F^4\gamma_{th}}{16(\xi_F^2+1)^2\overline{\gamma}_F}\middle|\begin{matrix}\frac{1}{2}-n,\frac{\xi_F^2+1}{2},\frac{\xi_F^2+2}{2}\\ \frac{\xi_F^2}{2},\frac{\xi_F^2+1}{2},\frac{\alpha_F}{2},\frac{\alpha_F+1}{2},\frac{\beta_F}{2},\frac{\beta_F+1}{2},-n-\frac{1}{2}\end{matrix}\right) \end{aligned} \tag{29}$$

$$\begin{aligned} I_{22}=&\frac{2^{\alpha_F+\beta_F-4}A\xi_F^2}{\pi^{3/2}\Gamma(\alpha_F)\Gamma(\beta_F)\Gamma(m)}\left(\frac{m\gamma_{th}}{\overline{\gamma}_R}\right)^m \\ &\times\sum_{i=0}^{\infty}\frac{1}{i!}\left(\frac{-m\gamma_{th}}{\overline{\gamma}_R}\right)^i\sum_{j=0}^{m+i-1}\binom{m+i-1}{j}(-1)^j \\ &\times G_{2,3}^{3,0}\left(B^2\gamma_{th}\middle|\begin{matrix}1,1-m-i+j\\ -m-i+j,0,\frac{1}{2}\end{matrix}\right) \\ &\times G_{3,7}^{6,1}\left(\frac{\alpha_F^2\beta_F^2\xi_F^4\gamma_{th}}{16(\xi_F^2+1)^2\overline{\gamma}_F}\middle|\begin{matrix}1-j,\frac{\xi_F^2+1}{2},\frac{\xi_F^2+2}{2}\\ \frac{\xi_F^2}{2},\frac{\xi_F^2+1}{2},\frac{\alpha_F}{2},\frac{\alpha_F+1}{2},\frac{\beta_F}{2},\frac{\beta_F+1}{2},-j\end{matrix}\right) \end{aligned} \tag{30}$$

therefore, I_2 can be obtained by substituting (8), (28), (29) and (30) into (27), and then substituting the derived I_1 and I_2 into (24) to obtain the average BER $\overline{P}_{e,AC}$ of the first hop S-R hybrid FSO/RF communication system based on adaptive combining scheme.

The average BER of the second hop R-D THz link is given as

$$\overline{P}_{e,T}=\int_0^{\infty}\frac{A}{2}\mathrm{erfc}(\sqrt{x}B)f_{\gamma_T}(x)\,\mathrm{d}x \tag{31}$$

substituting (14) in (31), and obtain

$$\begin{aligned} \overline{P}_{e,T}=&\frac{A\xi_T^{\xi_T^2}\mu^{\frac{\xi_T^2}{\alpha}}}{2\sqrt{\pi}A_{0,T}^{\xi_T^2}\Omega^{\xi_T^2}\Gamma(\mu)\overline{\gamma}_T^{\frac{\xi_T^2}{2}}}\frac{2^{\frac{\alpha\mu-\xi_T^2}{\alpha}-\frac{1}{2}}\alpha^{\frac{\xi_T^2}{2}-1}}{(2\pi)^{\frac{\alpha}{2}}B^{\frac{\xi_T^2}{2}}} \\ &\times G_{2+2\alpha,4+\alpha}^{4,2\alpha}\left(\frac{\mu^2\alpha^{\alpha}}{4B^{\alpha}A_{0,T}^{2\alpha}\Omega^{2\alpha}\overline{\gamma}_T^{\alpha}}\middle|\begin{matrix}\frac{1-\xi_T^2/2}{\alpha},\cdots,\frac{\alpha-\xi_T^2/2}{\alpha},\frac{1-\xi_T^2/2-1/2}{\alpha},\cdots,\frac{\alpha-\xi_T^2/2-1/2}{\alpha},\frac{1}{2},1\\ 0,\frac{1}{2},\frac{\alpha\mu-\xi_T^2}{2\alpha},\frac{\alpha\mu-\xi_T^2+1}{2\alpha},\frac{1-\xi_T^2/2-1}{\alpha},\cdots,\frac{\alpha-\xi_T^2/2-1}{\alpha}\end{matrix}\right) \end{aligned} \tag{32}$$

Considering DF relay, the E2E average BER of hybrid FSO/RF-THz relay communication system can be written as

$$\overline{P}_e=\overline{P}_{e,AC}+\overline{P}_{e,T}-2\times\overline{P}_{e,AC}\times\overline{P}_{e,T} \tag{33}$$

thus, the average BER of the system can be derived by substituting the obtained (24) and (32) into (33).

IV. Simulation Results

In order to analyze the performance of the hybrid FSO/RF-

TABLE I
SIMULATION PARAMETER SETTINGS

FSO link		RF link		THz link	
Parameters	Value	Parameters	Value	Parameters	Value
Wavelength λ_F	1550 nm			Carrier frequency f_T	300 GHz
Photoelectric. conversion η	1	Carrier frequency f_R	28 GHz	Link distance L_T	100 m
Strong turbulence C_n^2	1×10^{-12} m$^{-2/3}$	Link distance L_R	500 m	Transmit antenna gain $G_{t,T}$	55 dBi
Moderate turbulence C_n^2	1×10^{-13} m$^{-2/3}$	Transmit antenna gain $G_{t,R}$	44 dBi	Receive antenna gain $G_{r,T}$	55 dBi
Turbulence coefficient (strong) α_F, β_F	4.7206, 1.2066	Receive antenna gain $G_{r,R}$	44 dBi	Humidity ϕ	50%
Turbulence coefficient (moderate) α_F, β_F	5.6137, 4.0062	Oxygen absorption α_{oxy}	15.1 dB/km	Atmosphere pressure p	101325 Pa
Link distance L_F	500 m	Rain attenuation α_{rain}	0 dB/km	Temperature T	296 K
Receiving aperture r_a	20 cm			Jitter standard deviation $\sigma_{j,T}$	5 cm-15 cm
Jitter standard deviation $\sigma_{j,F}$	5 cm-20 cm				

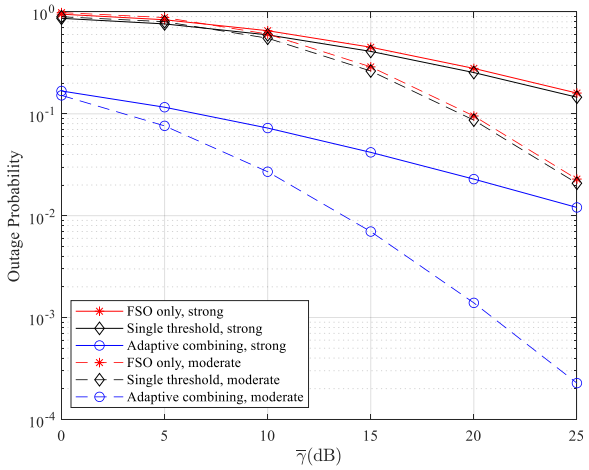

Fig. 2. Outage performance comparison of adaptive combining scheme, single-threshold switching scheme and single-link FSO system.

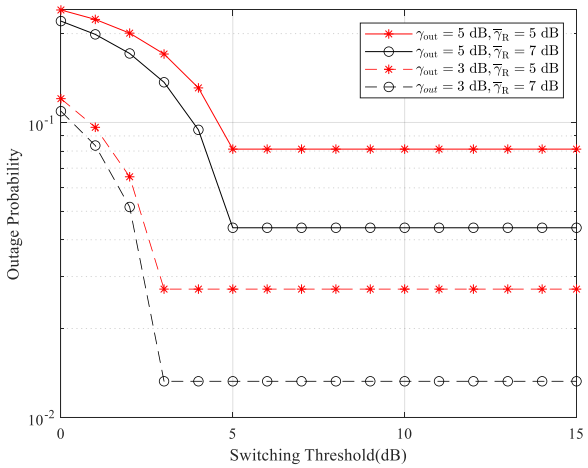

Fig. 3. The relationship between the outage probability and the switching threshold of the adaptive combining scheme.

THz relay system and verify the accuracy of the analysis results, simulations are performed based on the outage probability and BER expressions derived in Section 3, and the system simulation parameter settings are shown in Table 1. Assuming that the average SNR of the FSO link in Fig. 2 - 4 and 8 is $\bar{\gamma}_F=\bar{\gamma}$, Fig. 2 - 4 and 8 investigate the outage probability and BER performance of the first hop S-R hybrid FSO/RF system based on adaptive combining scheme in the hybrid FSO/RF-THz relay system; and assuming that the average SNR of FSO, RF and THz link in Fig. 5 - 7 and Fig. 9- 10 is $\bar{\gamma}_F=\bar{\gamma}_R=\bar{\gamma}_T=\bar{\gamma}$, the performance of hybrid FSO/RF-THz relay system under the influence of different parameters is studied in Fig. 5 - 7 and Fig. 9 - 10.

Fig. 2 compares the outage performance of single-link FSO, single-threshold switching scheme and adaptive combining scheme under moderate and strong turbulence conditions, considering m=1, $\bar{\gamma}_R$=8 dB , $\xi_F=4.5747$, γ_{th}=10 dB , γ_{out}=3 dB . It can be seen from Fig. 2 that compared with moderate turbulence, the outage probability of the system under strong turbulence conditions increases, indicating that the increase of turbulence intensity will lead to the deterioration of the outage performance of the system. At the same time, it can be observed from Fig. 2 that the outage performance of the adaptive combining scheme system is better than that of the single-link FSO and single-threshold switching scheme. The main reason for this phenomenon is that when the quality of the FSO link deteriorates, the single-link FSO has no backup link and can only use the FSO link for transmission all the time, while the single-threshold switching scheme can activate the RF link for transmission at this time, but there may be frequent link switching, which reduces the system transmission performance. The adaptive combining scheme overcomes the drawbacks of both, so it has better system performance.

Fig. 3 shows the relationship curve between the outage probability and the switching threshold of the adaptive

This article has been accepted for publication in IEEE Photonics Journal. This is the author's version which has not been fully edited and content may change prior to final publication. Citation information: DOI 10.1109/JPHOT.2024.3353194

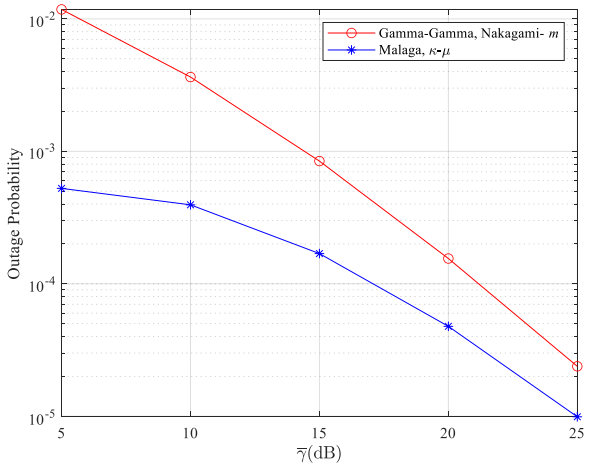

Fig. 4. The outage performance of the adaptive combining scheme under different distributions.

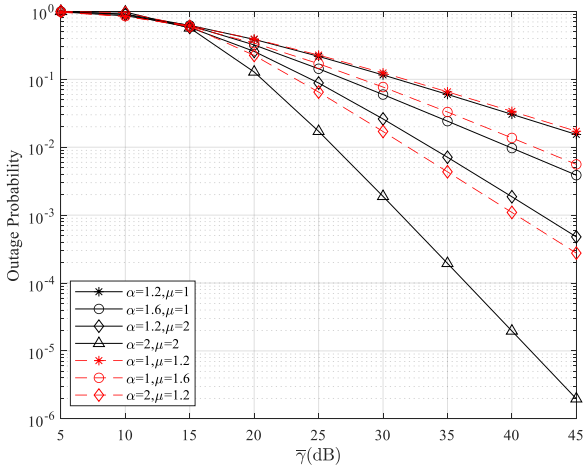

Fig. 5. The outage probability of the system under the influence of different fading parameters.

combining scheme, considering C_n^2=1×10^{-12} m$^{-2/3}$ (moderate turbulence), m=2, $\bar{\gamma}_F$=10 dB , $\xi_F = 4.5747$. It can be seen from Fig. 3 that when $\gamma_{th} < \gamma_{out}$, the system outage probability gradually decreases with the increase of the switching threshold; when $\gamma_{th} \geq \gamma_{out}$, the system outage probability reaches the minimum value, and at this point, the outage probability is a constant value. Therefore, in order to obtain the optimal outage performance, the switching threshold should be set higher than the outage threshold. At the same time, increasing the average SNR $\bar{\gamma}_R$ of the RF link can improve the system outage performance. This is because as $\bar{\gamma}_R$ increases, the RF link quality increases, thus providing a better quality backup link for the FSO link.

Fig. 4 illustrates the outage performance of the first-hop hybrid FSO/RF system based on the adaptive combining scheme with different FSO and RF distributions, assuming C_n^2=1×10^{-12} m$^{-2/3}$ (moderate turbulence), m=3, $\bar{\gamma}_R$=8 dB , $\xi_F = 4.5747$, γ_{th}=10 dB , γ_{out}=3 dB .In addition, the parameter value settings of Malaga distribution and κ-μ distribution in Fig. 4 can be referred to [33]. From Fig. 4, it can be seen that whether the FSO and RF channels follow the Gamma-Gamma distribution and Nakagami-m respectively, or the Malaga distribution and the κ-μ distribution, the adaptive combining scheme can significantly improve the outage performance of the system.

Fig. 5 shows the relationship curve between the average SNR and the hybrid FSO/RF-THz outage probability under different fading parameters, considering C_n^2=1×10^{-12} m$^{-2/3}$ (moderate turbulence), $\xi_F = 4.5747$, $\xi_T = 3.4450$, m=1, γ_{out}=5 dB . It can be seen from Fig. 5 that as the values of α and μ increase, the fading severity of the THz link decreases, resulting in an improvement in the outage performance of the system. In addition, the outage performance of the system under the two sets of parameter settings of {α=1.2, μ=1},

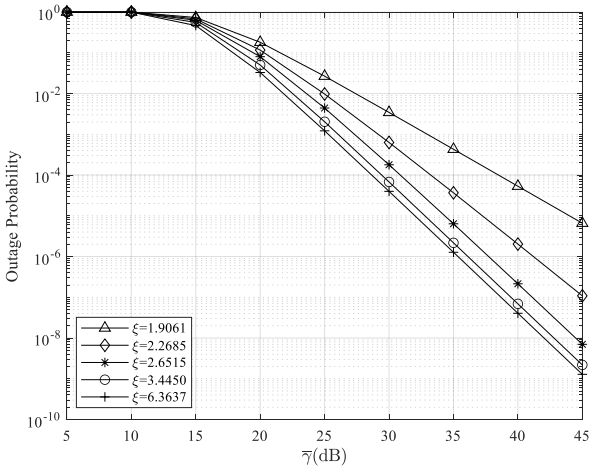

Fig. 6. The outage probability of the system under the influence of different pointing errors.

{α=1.6,μ=1}, {α=2,μ=1} and {α=1,μ=1.2}, {α=1,μ=1.6}, {α=1.2,μ=2} is compared respectively. It can be observed that when the degree of fading is comparable, the outage probability of the system when α>μ is lower than that when α<μ.

Fig. 6 shows the curves of the average SNR versus the outage probability of the hybrid FSO/RF-THz under different pointing errors, assuming $\xi_F = \xi_T = \xi$, C_n^2=1×10^{-12} m$^{-2/3}$ (moderate turbulence), m=1, α=3, μ=2, γ_{out}=5 dB . From Fig. 6, it can be seen that the smaller the value of pointing error ξ , the greater the impact on the system, resulting in a higher outage probability of the system, so increasing the pointing error can improve the outage performance of the system. However, when the pointing error increases to a certain value, continuing to increase the value of the pointing error does not have a significant effect on improving the outage performance of the system.

Fig. 7 depicts the relationship between the outage probability and the average SNR, the outage performance of

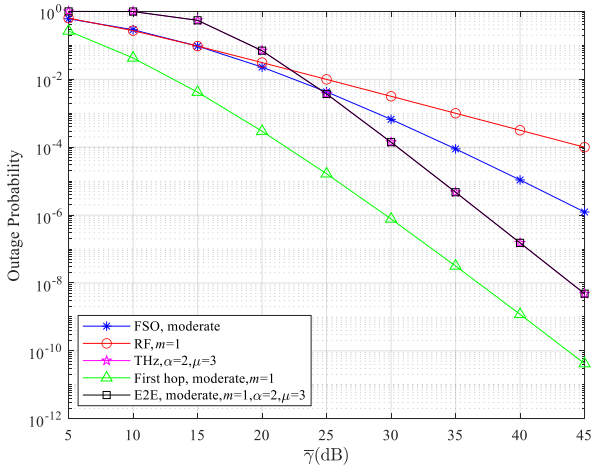

Fig. 7. The relationship between system outage probability and average SNR.

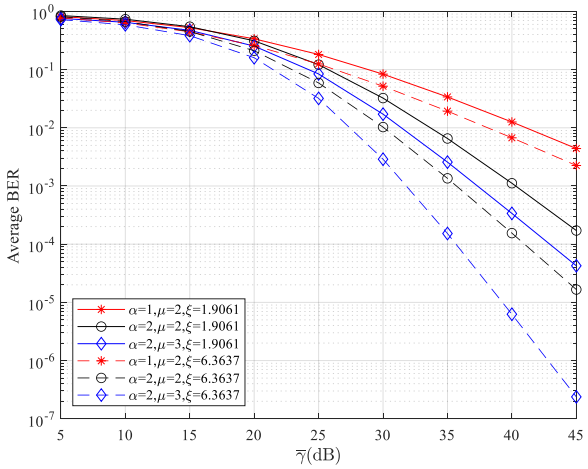

Fig. 9. The average BER of the system under the influence of different fading parameters and pointing errors.

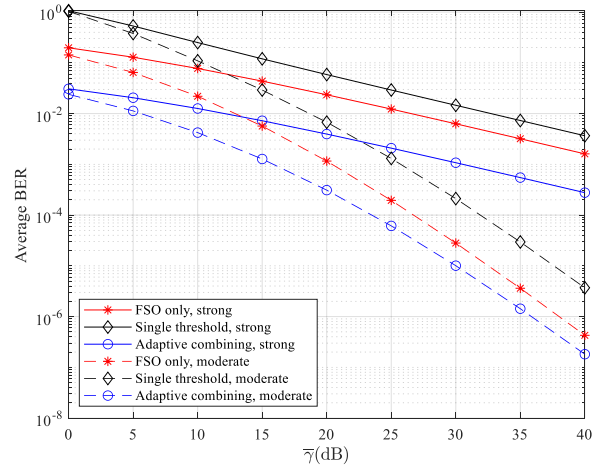

Fig. 8. Comparison of adaptive combining scheme with single-threshold switching scheme and single-link FSO BER performance.

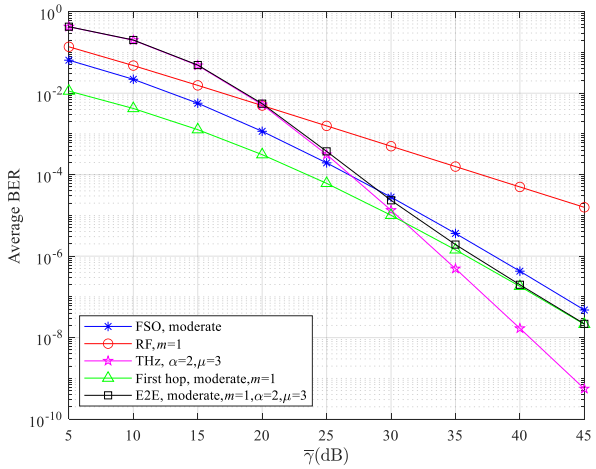

Fig. 10. The relationship between system average BER and average SNR.

FSO link, RF link, THz link, first hop adaptive combining hybrid FSO/RF system and E2E hybrid FSO/RF-THz relay system are studied, considering $\xi_F = 4.5747$, $\xi_T = 3.4450$, γ_{out}=5 dB. It can be seen from Fig. 7 that the outage performance of the THz link is the worst in the low SNR region. With the increase of the average SNR, the quality of the THz link is continuously improved. In the high SNR region, the outage performance of the THz link is better than that of the FSO link and the RF link. At the same time, it can be seen from (20) that the outage probability of the dual-hop relay system is determined by the hop with poor outage performance. Therefore, the outage performance of the E2E hybrid FSO/RF-THz relay system in Fig. 7 is basically consistent with that of the second hop THz link.

Fig. 8 compares the BER performance of single-link FSO, single-threshold switching scheme and adaptive combining scheme systems under moderate and strong turbulence conditions, considering M=2, m=1, $\bar{\gamma}_R$=5 dB, $\xi_F = 4.5747$, γ_{th}=7 dB. From Fig. 8, it can be seen that reducing the turbulence intensity of the FSO link can effectively improve the BER performance of the system. At the same time, it is also observed that the BER performance of the adaptive combining scheme system is better than that of the single-link FSO and single-threshold switching scheme under both moderate and strong turbulence conditions.

Fig. 9 shows the relationship between the average SNR and the BER of the hybrid FSO/RF-THz under different fading parameters and pointing errors, assuming $\xi_F = \xi_T = \xi$, $C_n^2 = 1 \times 10^{-12}$ m$^{-2/3}$ (moderate turbulence), M=2, m=1, γ_{th}=7 dB .From Fig. 9, it can be seen that the pointing error parameters ξ of FSO link and THz link, as well as the fading parameters α and μ of THz link, all have an impact on the BER performance of the system. The smaller the values of α, μ or ξ, the more serious the fading and pointing error of the system are. Increasing the value of α, μ or ξ can reduce the BER of the system and improve the communication quality of the system.

Fig. 10 shows the average BER versus the average SNR of the system, and the BER performance of FSO link, RF link, THz link, first hop adaptive combining hybrid FSO/RF system and E2E hybrid FSO/RF-THz relay system is studied, considering M=2, $\xi_{\mathrm{F}} = 4.5747$, $\xi_{\mathrm{T}} = 3.4450$, γ_{th}=7 dB . As can be seen in Fig. 10, in the low SNR region, the BER performance of the E2E hybrid FSO/RF-THz relay system remains consistent with that of the THz link until it enters the high SNR region, where the BER performance of the E2E hybrid FSO/RF-THz relay system is constantly approaching to that of the first hop adaptive combining hybrid FSO/RF system until the two are basically overlapped, which verifies the accuracy of (33).

V. Conclusion

This paper designs a hybrid FSO/RF-THz relay communication system, which uses a hybrid FSO/RF communication based on adaptive combining as the backhaul network before the relay node, and then connects to users through the THz link, which provides users with safe, reliable, low latency, and high-speed data transmission. Considering atmospheric turbulence and pointing errors in the FSO link, and fading and pointing errors in the THz link, the performance formulas of the hybrid FSO/RF-THz communication system are derived using the obtained statistical characteristics of the three links, FSO, RF, and THz. The simulation results show that compared with the single-threshold switching scheme and the single-link FSO system, the adaptive combining scheme in the first hop of the relay system can provide better system performance, and the optimal switching threshold of the adaptive combining scheme is obtained. At the same time, by evaluating the performance of the hybrid FSO/RF-THz relay system under different fading conditions and pointing errors, it is found that both channel fading and pointing errors will reduce the system performance; in addition, in the high SNR region, the hybrid FSO/RF-THz relay system can provide better outage and BER performance.

References

[1] R. Samy, H. C. Yang, T. Rakia, and M. S. Alouini, "Space-air-ground FSO networks for high-throughput satellite communications," *IEEE Commun. Mag.*, vol. 60, no. 12, pp. 82-87, Sep. 2022, doi: 10.1109/MCOM.002.2200018.

[2] E. Zedini, H. Soury, and M. S. Alouini, "On the performance analysis of dual-hop mixed FSO/RF systems," *IEEE Trans. Wireless Commun.*, vol. 15, no. 5, pp. 3679-3689, Feb. 2016, doi: 10.1109/TWC.2016.2524685.

[3] W. Fawaz, C. Abou-Rjeily, and C. Assi, "UAV-aided cooperation for FSO communication systems," *IEEE Commun. Mag.*, vol. 56, no. 1, pp. 70-75, Jan. 2018, doi: 10.1109/MCOM.2017.1700320.

[4] M. Z. Chowdhury, M. K. Hasan, M. Shahjalal, M. T. Hossan, and Y. M. Jang, "Optical wireless hybrid networks: Trends, opportunities, challenges, and research directions," *IEEE Commun. Surveys Tuts.*, 2020, 22(2): 930-966. vol. 22, no. 2, pp. 930-966, Jan. 2020, doi: 10.1109/COMST.2020.2966855.

[5] P. Bhardwaj and S. M. Zafaruddin, "On the performance of multihop THz wireless system over mixed channel fading with shadowing and antenna misalignment," *IEEE Trans. Commun.*, vol. 70, no. 11, pp. 7748-7763, Sep. 2022, doi: 10.1109/TCOMM.2022.3205657.

[6] M. Zhu et al., "Ultra-wideband fiber-THz-fiber seamless integration communication system toward 6G: architecture, key techniques, and testbed implementation," *Sci. China Inf. Sci.*, vol. 66, no. 1, pp. 1-18, Dec. 2022, doi: 10.1007/s11432-022-3565-3.

[7] E. Zedini, I. S. Ansari, and M. S. Alouini, "Performance analysis of mixed Nakagami-*m* and Gamma–Gamma dual-hop FSO transmission systems," *IEEE Photon. J.*, vol. 7, no. 1, pp. 1–20, Feb. 2015, doi: 10.1109/JPHOT.2014.2381657.

[8] L. Yang, W. Guo, and I. S. Ansari, "Mixed dual-hop FSO-RF communication systems through reconfigurable intelligent surface," *IEEE Commun. Lett.*, vol. 24, no. 7, pp. 1558-1562, Jul. 2020, doi: 10.1109/LCOMM.2020.2986002.

[9] B. Ashrafzadeh, E. Soleimani-Nasab, M. Kamandar, and M. Uysal, "A framework on the performance analysis of dual-hop mixed FSO-RF cooperative systems," *IEEE Trans. Commun.*, vol. 67, no. 7, pp. 4939-4954, Jul. 2019, doi: 10.1109/TCOMM.2019.2904501.

[10] L. Qu, G. Xu, Z. Zeng, N. Zhang, and Q. Zhang, "UAV-assisted RF/FSO relay system for space-air-ground integrated network: A performance analysis," *IEEE Trans. Wireless Commun.*, vol. 21, no. 8, pp. 6211-6225, Aug. 2022, doi: 10.1109/TWC.2022.3147823.

[11] G. Xu and Z. Song, "Performance analysis for mixed κ-μ fading and M-distribution dual-hop radio frequency/free space optical communication systems," *IEEE Trans. Wireless Commun.*, vol. 20, no. 3, pp. 1517-1528, Mar. 2021, doi: 10.1109/TWC.2020.3034104.

[12] S. Li et al., "Mixed THz/FSO relaying systems: Statistical analysis and performance evaluation," *IEEE Trans. Wireless Commun.*, vol. 21, no. 12, pp. 10996-11010, Jul. 2022, doi: 10.1109/TWC.2022.3188698.

[13] P. Bhardwaj amd S. M. Zafaruddin, "Performance of hybrid THz and multiantenna RF system with diversity combining," *IEEE Syst. J.*, vol. 17, no. 2, pp. 2546-2557, Nov. 2022, doi: 10.1109/JSYST.2022.3203797.

[14] B. He and R. Schober, "Bit-interleaved coded modulation for hybrid RF/FSO systems," *IEEE Trans. Commun.*, vol. 57, no. 12, pp. 3753-3763, Dec. 2009, doi: 10.1109/TCOMM.2009.12.080396.

[15] M. A. Amirabadi and V. T. Vakili, "A novel hybrid FSO/RF communication system with receive diversity," *Optik*, vol. 184, pp. 293-298, Mar. 2019, doi: 10.1016/j.ijleo.2019.03.037.

[16] W. M. R. Shakir, "Performance evaluation of a selection combining scheme for the hybrid FSO/RF system," *IEEE Photon. J.*, vol. 10, no. 1, pp. 1-10, Nov. 2017, doi: 10.1109/JPHOT.2017.2771411.

[17] F. Nadeem et al., "Weather effects on hybrid FSO/RF communication link," *IEEE J. Sel. Areas Commun.*, vol. 27, no. 9, pp. 1687-1697, Dec. 2009, doi: 10.1109/JSAC.2009.091218.

[18] A. AbdulHussein, A. Oka, T. T. Nguyen, and L. Lampe, "Rateless coding for hybrid free-space optical and radio-frequency communication," *IEEE Trans. Wireless Commun.*, vol. 9, no. 3, pp. 907-913, Mar. 2010, doi: 10.1109/TWC.2010.03.090108.

[19] M. Usman, H. C. Yang, and M. S. Alouini, "Practical switching-based hybrid FSO/RF transmission and its performance analysis," *IEEE Photon. J.*, vol. 6, no. 5, pp. 1-13, Aug. 2014, doi: 10.1109/JPHOT.2014.2352629.

[20] T. Rakia, H. C. Yang, M. S. Alouini, and F. Gebali, "Outage analysis of practical FSO/RF hybrid system with adaptive combining," *IEEE Commun. Lett.*, vol. 19, no. 8, pp. 1366-1369, Aug. 2015, doi: 10.1109/LCOMM.2015.2443771.

[21] S. Magidi and A. Jabeena, "Analysis of hybrid FSO/RF communication system under the effects of combined atmospheric fading and pointing errors," *Opt. Quantum Electron.*, vol. 54, no. 4, pp. 1-20, Mar. 2022, doi: 10.1007/s11082-022-03586-y.

[22] W. A. Alathwary and E. S. Altubaishi, "On the performance analysis of decode-and-forward multi-hop hybrid FSO/RF systems with hard-switching configuration," *IEEE Photon. J.*, vol. 11, no. 6, pp. 1–12, Dec. 2019, doi: 10.1109/JPHOT.2019.2949859.

[23] Y. Wu, J. Chen, J. Guo, G. Li, and D. Kong, "Performance analysis of a multi-hop parallel hybrid FSO/RF system over a Gamma–Gamma turbulence channel with pointing errors and a Nakagami-*m* fading channel," *Photonics*, vol. 9, no. 9, pp. 631-645, Sep. 2022, doi: 10.3390/photonics9090631.

[24] S. Shah, M. Siddharth, N. Vishwakarma, R. Swaminathan, and A. S. Madhukumar, "Adaptive-combining-based hybrid FSO/RF satellite communication with and without HAPS," *IEEE Access*, vol. 9, pp. 81492-81511, Jun. 2021, doi: 10.1109/ACCESS.2021.3086024.

[25] R. Boluda-Ruiz, A. Garc á-Zambrana, C. Castillo-V ázquez, and B. Castillo-V ázquez, "Novel approximation of misalignment fading modeled by Beckmann distribution on free-space optical links," *Opt. Exp.*, vol. 24, no. 20, pp. 22635-22649, Sep. 2016, doi:

10.1364/OE.24.022635.

[26] G. T. Djordjevic, M. I. Petkovic, A. M. Cvetkovic, and G. K. Karagiannidis, "Mixed RF/FSO relaying with outdated channel state information," *IEEE J. Sel. Areas Commun.*, vol. 33, no. 9, pp. 1935-1948, May. 2015, doi: 10.1109/JSAC.2015.2433055.

[27] A. Touati, A. Abdaoui, F. Touati, M. Uysal, and A. Bouallegue, "On the effects of combined atmospheric fading and misalignment on the hybrid FSO/RF transmission," *J. Opt. Commun. Networking*, vol. 8, no. 10, pp. 715-725, Sep. 2016, doi: 10.1364/JOCN.8.000715.

[28] S. Sharma, A. S. Madhukumar, and R. Swaminathan, "Effect of pointing errors on the performance of hybrid FSO/RF networks," *IEEE Access*, vol. 7, pp. 131418-131434, Sep. 2019, doi: 10.1109/ACCESS.2019.2940630 .

[29] S. Li and L. Yang, "Performance analysis of dual-hop THz transmission systems over α-μ fading channels with pointing errors," *IEEE Internet Things J.*, vol. 9, no. 14, pp. 11772-11783, Dec. 2021, doi: 10.1109/JIOT.2021.3131978.

[30] S. Li, Y. Yang, L. Yang, and Y. Bian, "On the study of multiuser mixed dual-hop RF/THz systems," *IEEE Trans. Veh. Technol.*, vol. 72, no. 7, pp. 9175-9188, Mar. 2023, doi: 10.1109/TVT.2023.3251349.

[31] M. Siddharth, S. Shah, N. Vishwakarma, and R. Swaminathan, "Performance analysis of adaptive combining based hybrid FSO/RF terrestrial communication," *IET Commun.*, vol. 14, no. 22, pp. 4057-4068, Feb. 2021, doi: 10.1049/iet-com.2020.0598.

[32] P. K. Singya, B. Makki, A. D'Errico, and M. S. Alouini, "Hybrid FSO/THz-based backhaul network for mmWave terrestrial communication," *IEEE Trans. Wireless Commun.*, vol. 22, no. 7, pp. 4342-4359, Dec. 2022, doi: 10.1109/TWC.2022.3224331.

[33] N. Vishwakarma and R. Swaminathan, "On the capacity performance of hybrid FSO/RF system with adaptive combining over generalized distributions," *IEEE Photon. J.*, vol. 14, no. 1, pp. 1-12, Feb. 2021, doi: 10.1109/JPHOT.2021.3135115.